Contents

Part I

Preliminaries

Chapter 1

RBF Methods for PDEs

The process of solving partial differential equations (PDEs) using radial basis functions (RBFs) dates back to 1990 [36, 37]. However, at the core of all RBF methods lies the fundamental problem of approximation/interpolation. Some methods (e.g., global- and compact-RBF methods) apply RBFs to approximate derivatives directly. Others (e.g., RBF-generated Finite Differences) leverage the basis functions to generate weights for finite-differencing stencils, utilizing the weights in turn to approximate derivatives. Regardless, to track the history of RBF methods, one must look back to 1971 and R.L. Hardy's seminal research on interpolation with multi-quadric basis functions [32].

As "meshless" methods, RBF methods excel at solving problems that require geometric flexibility with scattered node layouts in d-dimensional space. They naturally extend into higher dimensions without significant increase in programming complexity [21, 60]. In addition to competitive accuracy and convergence compared with other state-of-the-art methods [18, 19, 21, 22, 60], they also boast stability for large time steps.

This chapter is dedicated to summarizing the four-decade history of RBF methods leading up to the development of the RBF-generated Finite Differences (RBF-FD) method. Beginning with a brief introduction to RBFs and a historical survey, we attempt to classify related work into three three types: global, compact, and local methods. Following this, the general approximation problem is introduced, with a look at the core of all three method classificiations: RBF scattered-data interpolation.

Three global RBF collocation methods are presented: Kansa's method, Fasshauer's method and Direct collocation. Within the historical context of RBF methods we highlight extensions that lead to local interpolation matrices instead of a single global interpolation matrix. Additionally, the RBF-pseudospectral (RBF-PS) method is shown as an extension to fit global RBF methods into the framework of lower complexity pseudo-spectral methods.

By surveying related work in the field of RBF PDE methods, we frame the context in which RBF-FD was developed, and illustrate both the benefits and pitfalls inherited from its predecessors.

1.1 Survey of Related Work

In Radial Basis Function methods, radially symmetric functions provide a non-orthogonal basis used to interpolate between nodes of a point cloud. RBFs are univariate and a function of distance from a center point defined in $\mathbb{R}^d$, so they easily extend into higher dimensions without significant change in programming complexity. Examples of commonly used RBFs from the literature are provided in Table 1.1; 2D representations of the same functions can be found in Figure 1.1. Figure 1.2 illustrates the radial symmetry of RBFs—in this case, a Gaussian RBF—in the first three dimensions.

RBF methods are based on a superposition of translates of these radially symmetric functions, providing a linearly independent but non-orthogonal basis used to interpolate between nodes in d-dimensional space. The interpolation problem—referred to as *RBF scattered data interpolation*—seeks the unknown coefficients, $\mathbf{c} = \{c_j\}$, that satisfy:

$$\sum_{j=1}^{N} \phi_j(r(\mathbf{x}))c_j = f(\mathbf{x}),$$

where $\phi_j(r(\mathbf{x}))$ is an RBF centered at $\{\mathbf{x}_j\}_{j=1}^{n}$. In theory the radial coordinate, $r(\mathbf{x})$, could be any distance metric, but is most often assumed to be $r(\mathbf{x}) = ||\mathbf{x} - \mathbf{x}_j||_2$ (i.e., Euclidean distance), as it is here. The coefficients $\mathbf{c}$ result in a smooth interpolant that collocates sample values $f(\mathbf{x}_j)$. An example of RBF interpolation in 2D using 15 Gaussians is shown in Figure 1.3.

RBFs have been shown in some cases to have exponential convergence for function approximation [15]. It is also possible to reformulate RBF methods as pseudospectral methods that have generated solutions to ill-posed problems for which Chebyshev-based and other pseudospectral methods fail [13]. However, as with all methods, RBFs come with certain limitations. For example, RBF interpolation is—in general—not a well-posed problem, so it requires careful choice of positive definite or conditionally positive definite basis functions (see [15, 35] for details).

RBFs depend on a shape or support parameter ϵ that controls the width of the function. The functional form of the shape function becomes $\phi(\epsilon \, r(\mathbf{x}))$. For simplicity in what follows, we use the notation $\phi_j(\mathbf{x})$ to imply $\phi(\epsilon||\mathbf{x} - \mathbf{x}_j||_2)$. Decreasing ϵ increases the support of the RBF and in most cases, the accuracy of the interpolation, but worsens the conditioning of the RBF interpolation problem [45]. This inverse relationship is widely known as the *Uncertainty Relation* [35, 45]. Fortunately, recent algorithms such as Contour-Padé [24] and RBF-QR [26, 28] allow for numerically stable computation of interpolants in the nearly flat RBF regime (i.e., $\epsilon \to 0$) where high accuracy has been observed [29, 39].

RBF methods for interpolation first appeared in 1971 with Hardy's seminal research on multiquadrics [32]. In his 1982 survey of scattered data interpolation methods [30], Franke rated multiquadrics first-in-class against 28 other methods (3 of which were RBFs) [30]. Many other RBFs, including those presented in Table 1.1 have been applied in literature, but for PDEs in particular, none have rivaled the attention received by multiquadrics.

By 1990, the understanding of the scientific community regarding RBFs was sufficiently

Name	Abbrev.	Formula	Order (m)
Multiquadric	MQ	$\sqrt{1 + (\varepsilon r)^2}$	1
Inverse Multiquadric	IMQ	$\frac{1}{\sqrt{1+(\varepsilon r)^2}}$	0
Gaussian	GA	$e^{-(\varepsilon r)^2}$	0
Thin Plate Splines	TPS	$r^2 ln|r|$	2
Wendland (C^2)	W2	$(1 - \varepsilon r)^4(4\varepsilon r + 1)$	0

Table 1.1: Examples of frequently used RBFs based on [15, 29]. ε is the support parameter. All RBFs have global support. For compact support, enforce a cut-off radius (see Equation 1.1).
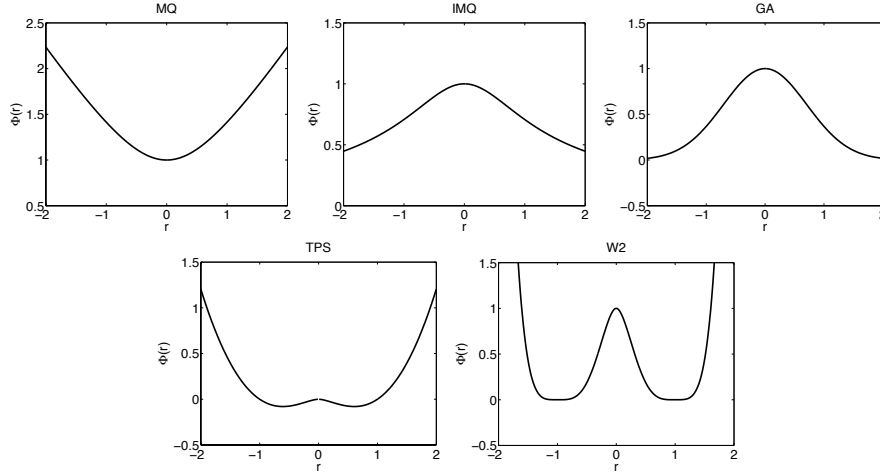
Figure 1.1: Example RBF shapes from Table 1.1 with parameter $\varepsilon = 1$.

developed for collocating PDEs [36, 37]. PDE collocation seeks a solution of the form

$$(\mathcal{L}u)(x_i) = \sum_{j=1}^{N} \phi_j(x_i)c_j = f(x_i)$$

where $\mathcal{L}$ is, in general, a nonlinear differential operator acting on $u(x)$. The solution $u(x)$ is expressed as a linear combination of N basis functions $\phi_j(x)$, not necessarily RBFs:

$$u(x) = \sum_{i=1}^{N} \phi_j(x)c_j$$

As in the problem of RBF scattered data interpolation, $\mathbf{c} = \{c_j\}$ is the unknown coefficient vector. Under the assumption that $\mathcal{L}$ is a linear operator, one can collocate the differential equation. Alternatively, individual derivative operators can be expressed as linear combinations of the unknowns u_j (leading to the RBF-FD methods). In all cases, a linear system

Figure 1.2: The Gaussian (GA) RBF (Table 1.1) with parameter $\varepsilon = 1$ and r in $D = 1$, 2 and 3.

Figure 1.3: RBF interpolation using 15 translates of the Gaussian RBF with $\epsilon = 2$. One RBF is centered at each node in the domain. Linear combinations of these produce an interpolant over the domain passing through known function values.
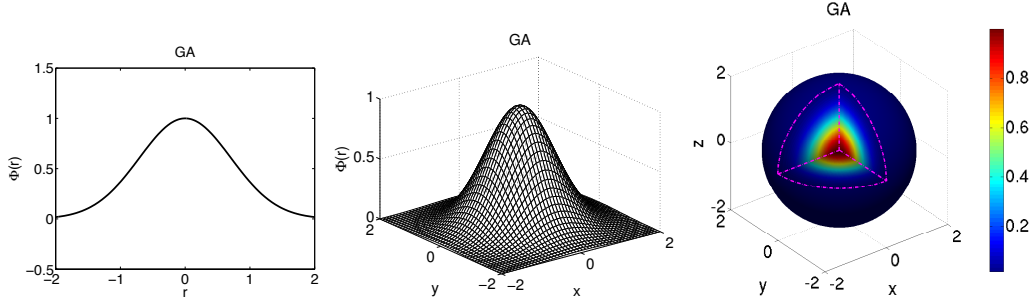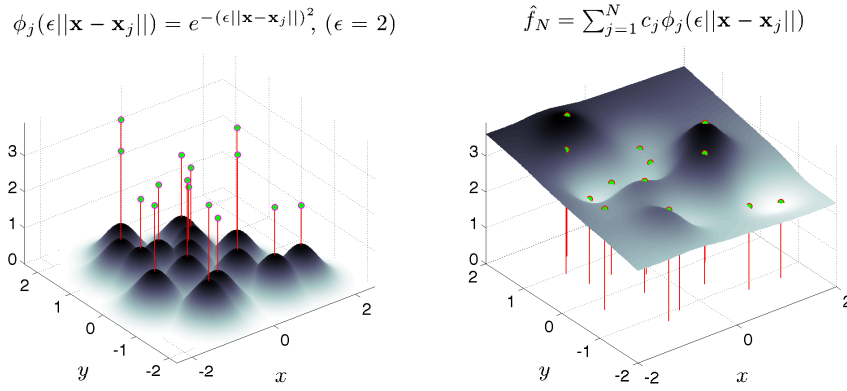
of equations arises, with different degrees of sparsity, dependent on the chosen basis functions and how the various constraints are enforced. While we restrict the $\phi_j(x)$ to RBFs or various operators applied to the RBFs, we note that spectral methods, finite-element or spectral-element methods can be formulated in a similar way with different choices of basis functions. Of course, u can be a vector of unknown variables (**c** then becomes a matrix).

In Table 1.3 we classify references according to their choice of collocation method and RBF interpolation type. There are three main categories of RBF interpolation; we list them in Table 1.2. The first is *Global* in the case that a single, large ($N \times N$) and dense matrix corresponding to globally supported RBFs is inverted; second, *Compact* if compactly supported RBFs are used to produce a single, large, but *sparse* matrix; and third, *Local* if compactly supported RBFs are used to produce many small but dense matrices with one corresponding to each collocation point. In all three cases the matrices are symmetric and with the correct choice of RBF they are at least conditionally positive definite. The final row of Table 1.3 considers literature on the RBF-FD method and is discussed in depth in Chapter 2.

We note that three types of collocation occur throughout the RBF literature: Kansa's unsymmetric collocation method [36, 37], Fasshauer's symmetric collocation method [14], and the Direct collocation method [17].

6

Interpolation Type	Dense/Sparse A	$\text{Dim}(A)$ ($N_S \ll N$)	# of A^{-1}	RBF Support
Global	Dense	$N \times N$	1	Global
Compact	Sparse	$N \times N$	1	Compact
Local	Dense	$N_S \times N_S$	N	Global/Compact

Table 1.2: RBF interpolation types and properties, assuming a problem with N nodes.

We now turn to discussion of the benefits and shortcomings of each RBF method, before covering derivation of the methods.

1.1.1 Global RBF Methods

Kansa's method [36, 37] (a.k.a. unsymmetric collocation) was the first RBF method for PDEs, and is still the most frequently used method. The idea behind Kansa's method is that an approximate solution to the PDE can be found by finding an interpolant which satisfies the differential operator with zero residual at a set of *collocation points* (these coincide with the RBF centers). To find the interpolant, the differential equation is formulated as a two block (unsymmetric) linear system with: 1) the approximation of values at boundary points with boundary data only, and 2) the approximation of interior points by directly applying the differential operator. It was shown in [14, 33] that the unsymmetric linear system produced by Kansa's method does not guarantee non-singularity; although it is also noted that in practice singularities are rare encounters [39].

The second alternative for RBF collocation, is based on Hermite scattered data interpolation (see [62]). The so-called *Fasshauer* or *Symmetric Collocation* method ([14]) performs a change of basis for the interpolant by directly applying the differential operator to the RBFs. It then collocates using the same approach as Kansa's method [39, 50]. The resulting block structure of the linear system is symmetric and guaranteed to be non-singular [14]. In comparison to Kansa's method, the disadvantages of Fasshauer's method include: a) requirement of higher order differentiability of the basis functions (to satisfy double application of the differential operator) and b) the linear system is larger and more complex to form [15]. As [33] points out, the possible existence of a singularity in Kansa's method is not enough to justify the added difficulties of using Fasshauer's method.

The last collocation method, *Direct Collocation*, was introduced by Fedoseyev, Friedman and Kansa [17] and satisfies the differential operator on the interior and the boundary. Larsson and Fornberg [39] observe that this third method has a matrix structure similar to that found in Kansa's method; however, it is noted that the dimensions of the matrix blocks for each method differ. This is due to collocation constraints added for the differential operator applied to the boundary. Aside from the survey on RBF collocation presented by Larsson and Fornberg [39], no related work was found that applied, or investigated, this method further.

Both Kansa's method and Fasshauer's methods were shown in [13] to fit well in the generalized framework of pseudo-spectral methods with a subtle change in algorithm. While

collocation methods explicitly compute the coefficients for a continuous derivative approximation, their alternates, referred to in literature as RBF-pseudospectral (RBF-PS) methods, never explicitly compute the interpolant coefficients. Instead, a differentiation matrix (DM) is assembled and used to approximate derivates at the collocation points only [16]. Since most computational models are simply concerned with the solution at collocation points, the change to assemble DMs as in RBF-PS is organic.

Following the evolution of the RBF-PS algorithm, applications of global RBFs in the classic collocation sense (i.e., without the RBF-PS DMs) become impractical. This statement stems from the algorithmic complexity of each method. Global RBF methods result in full matrices [15]. The global collocation methods then scale on the order of $O(N^3)$ floating point operations (FLOPs) to solve for weighting coefficients on a given node layout, plus $O(N^2)$ to apply the weights for derivatives. If time-stepping is required, global collocation methods must recompute the time-dependent coefficients with additional cost dominated by $O(N^3)$ operations. RBF-PS methods have similar requirements for $O(N^3)$ operations to assemble the differentiation matrix and $O(N^2)$ to apply for derivatives. However, by avoiding time-dependent coefficients, RBF-PS methods only apply the differentiation matrix each time-step for $O(N^2)$ operations. As an aside, the $O(N^3)$ complexity for each method—typically due to an LU-decomposition, with subsequent forward- and back-solves—could be reduced. While not in mainstream use by the RBF community, [42] correctly points out that the use of iterative solvers could reduce complexity of preprocessing to the order of $O(N^2)$.

Hon et al. [34] employed Kansa's method to solve shallow water equations for Typhoon simulation. In [22], Flyer and Wright employed RBF-PS (Kansa method) for the solution of shallow water equations on a sphere. Their results show that RBFs allow for longer time steps with spectral accuracy. The survey [18] by Flyer and Fornberg showcases RBF-PS (Kansa) out-performing some of the of the best available methods in geosciences, namely: Finite Volume, Spectral Elements, Double Fourier, and Spherical Harmonics. When applied to problems such as transport on the sphere [21], shallow water equations [22], and 3D mantle convection[60], RBF-PS consistently required fewer time steps, and a fraction of the nodes for similar accuracy [18].

1.1.2 Compactly Support RBFs

Thus far, all cases of collocation and interpolation mentioned have assumed globally supported RBFs. While global RBFs are well-studied and have nice properties, a major limitation is the large, dense system that must be solved. One alternative to global support is to use a set of compactly supported RBFs (CSRBFs) that are defined as:

$$\phi(r) = \begin{cases} \varphi(r) & r \in [0, 1] \\ 0 & r > 1 \end{cases} \tag{1.1}$$

where a cut-off radius is defined past which the RBF (in this case $\varphi(r)$) has no influence on the interpolant. Note that the radius can be scaled to fit a desired support. Methods that leverage CSRBFs produce a global interpolation matrix that is *sparse* and therefore results in a system that is more efficiently assembled and solved with smaller memory requirements [15]. The actual complexity estimate of the CSRBF method depends on the sparsity of the

8

| | RBF Interpolation Type | | |
Method	Global (Dense)	Compact (Sparse Global)	Local
Kansa's Method	[13, 18, 21, 22, 24, 29, 30, 33, 34, 36, 37, 39, 43, 47, 60]	[29, 57]	[12, 38, 55, 56]
Fasshauer's Method	[13, 14, 39]	[41]	[50, 51, 52]
Direct Collocation	[17, 39]		
RBF-FD	N/A	N/A	[7, 8, 11, 19, 20, 26, 27, 48, 49, 58, 59, 61]

Table 1.3: Classification of references based on choice of RBF interpolation types and method for solving PDEs. References may appear in multiple cells according to the breadth of their research.

problem as well as the ordering of the assembled system. Assuming $n \ll N$ where n represents the number of nodes in support, [65] lists the complexity as dominated by $O(N)$ for properly structured systems within MATLAB, and the investigation in [42] found $O(N^{1.5})$ consistent with the estimate provided by their choice of general sparse solver package. A multi-level CSRBF method, introduced by Fasshauer [15], collocates solutions over multiple grid refinements to achieve reduced $O(N)$ complexity, but the method is plagued by poor convergence. We also notes that in the context of CSRBFs, analogues to Kansa's method and Fasshauer's method are known by the names *radial point interpolation method (RPIM)* [57] and *radial point interpolation collocation method (RPICM)* [41], respectively. A more thorough survey of CSRBF history can be found in [15, 35].

CSRBFs have attracted a lot of attention in applications. For example, in the field of dynamic surface and image deformation, compact support allows for local transformations which do not induce global deformation (see e.g., [10, 40, 63]).

1.1.3 Local RBF Methods

Around 2005, Šarler and Vertnik [55, 56] demonstrated that if compactly supported RBFs are chosen, the traditional global collocation matrix from Kansa's method, can be avoided altogether in favor of small localized collocation matrices defined for each node. Local collocation still faces possible ill-conditioning and singularities like global collocation, but make it easier to distribute computation across parallel systems. Also, the smaller linear systems can be solved with less conditioning issues. In [56], the authors consider 2D diffusion problems. Divo and Kassab [12] employ the method for Poisson-like PDEs including fluid flow and heat transfer. Kosec and Šarler [38] apply the same technique to solve coupled heat transfer and fluid flow problems.

In similar fashion, Stevens et al. [52] introduced a local version of Fasshauer's method called *local Hermitian interpolation.* The authors have applied their method to 3D soil problems based on transient Richards' equations [50, 51, 52].

1.1.4 Recent Advances in Conditioning

The most limiting factor in the success of RBF methods is not the complexity of the methods, nor the task of collocating the PDE. Rather, it is the support parameter, ϵ, and the dilemma one faces in the *Uncertainty Relation* [45]. Recall that as $\epsilon \to 0$ ill-conditioning increases, but the accuracy of the method also increases. Similarly, as the number of collocation points increases, so too does the ill-conditioning.

In response to this problem, Fornberg and Wright [24] presented the *Contour–Padé algorithm*, which allows for numerically stable computation of highly accurate interpolants for (very small) cases typically associated with ill-conditioning induced by nearly flat RBFs (i.e., $\epsilon \to 0$). Larsson and Fornberg [39] applied the algorithm to all three methods of collocation (Kansa's, Fasshauer's and Direct Collocation) with considerable gain in accuracy over solutions from classical second-order FD and a pseudospectral method. Note that currently, the Contour-Padé algorithm was only studied for global RBF interpolation, not for compact or local collocation methods.

The *RBF-QR* method, an alternative for numerically stable computation in the limit as $\epsilon \to 0$, was introduced by Fornberg and Piret [28] in context of a sphere, and later extended to planar 2D problems in [25]. The RBF-QR method is simple to implement (less than 100 lines of Matlab code), and it allows solution of large problems that are typically ill-conditioned. Fornberg, Larsson and Flyer [25] successfully applied RBF-QR on large problems with 6000 nodes for globally supported basis functions.

With these two algorithms, global RBF methods have overcome most ill-conditioning issues for small to mid-sized problems. Unfortunately, both Contour-Padé and RBF-QR fail for large problems. As the number of RBFs increases beyond a few thousand nodes it is impossible to avoid ill-conditioning of the extremely large interpolation matrix.

This reveals the benefit of local methods, which decrease the number of RBFs and ill-conditioning. However, in the limit as local stencil size increases to include all nodes in a domain, the local and global method are equivalent; thus it is known that local methods also suffer extreme ill-conditioning around 2000 nodes per stencil [49]. Although, to our knowledge, no applications of local methods require more than a few hundred nodes per local solution.

1.2 Comparison of RBF Methods

We now detail RBF methods for PDEs leading up to the derivation of RBF-FD.

Following [43], consider a PDE expressed in terms of a (linear) differential operator, $\mathcal{L}$:

$$\begin{aligned} \mathcal{L}u &= f && \text{on } \Omega \\ u &= g && \text{on } \Gamma \end{aligned}$$

where Ω is the interior of the physical domain, Γ is the boundary of Ω and f, g are known explicitly. In the case of a non-linear differential operator, a Newton's iteration, or some

other method, can be used to linearize the problem (see e.g., [61]); of course, this increases the complexity of a single time step. Then, the unknown solution, u, which produces the observations on the right hand side can be approximated by an interpolant function u_ϕ expressed as a linear combination of radial basis functions, $\{\phi_j(x) = \phi(||x - x_j||)\}_{j=1}^N$, and polynomial functions $\{P_l(x)\}_{l=1}^M$:

$$u_\phi(x) = \sum_{j=1}^N \phi_j(x)c_j + \sum_{l=1}^M P_l(x)d_l, \quad P_l(x) \in \Pi_p^d \quad (1.2)$$

where $\phi_j(x) = ||x - x_j||_2$ (Euclidean distance). The second sum represents a linear combination of polynomials that enforces zero approximation error when $u(x)$ is a polynomial of degree less than or equal to p. The variable d is the problem dimension (i.e., $u_\phi(x) \in \mathbb{R}^d$). To eliminate degrees of freedom for well-posedness, p should be greater than or equal to the order of the chosen RBF (see Table 1.1) [35]. Note that Equation 1.2 is evaluated at $\{x_j\}_{j=1}^N$ data points through which the interpolant is required to pass with zero residual. We refer to the x_j's as *collocation points* (a.k.a. trial points), taken as the RBF centers. The test points, x, usually coincide with collocation points, although this is not a requirement.

To clarify the role of the polynomial part in Equation 1.2, it is necessary to put aside the PDE for the moment and consider only the problem of *scattered data interpolation* with Radial Basis Functions.

1.2.1   RBF Scattered Data Interpolation

Borrowing notation from [15, 35], we seek an interpolant of the form

$$f(x) = \sum_{j=1}^N \phi_j(x)c_j$$

where $f(x)$ is expressed as a scalar product between the unknown coefficient weights c_j and the radial basis functions $\phi_j(x)$.

To obtain the unknown coefficients, c_j, form a linear system in terms of the N RBF centers:

$$f(x) = \sum_{j=1}^N c_j\phi_j(x) \quad \text{for } x = \{x_j\}_{j=1}^N$$

$$(\ f\ ) = [\ \phi\ ](\ c\ )$$

The invertibility of this system depends on the choice of RBF, so one typically chooses a function that is positive definite to avoid issues. It has been shown (see [15, 35]) that some choices of RBFs (e.g. multiquadrics and thin-plate splines [33]) are not positive definite and therefore there is no guarantee that the approximation is well-posed. A sufficient condition for well-posedness is that the matrix be *conditionally positive definite*. In [15], Fasshauer demonstrates that conditional positive definiteness is guaranteed when Equation 1.2 exactly reproduces functions of degree less than or equal m. For RBF scattered data interpolation

11

in one dimension, this can be achieved by adding a polynomial of order m with $M = \binom{m+1}{1}$ terms (e.g., $x^0, x^1, \cdots, x^m$). In $\mathbb{R}^d$, $M = \binom{m+d}{d}$ [35], giving

$$\sum_{j=1}^{N} c_j \phi_j(x) + \sum_{l=1}^{M} d_l P_l(x) \quad = \quad f(x), \qquad P_l(x) \in \Pi_m^d \tag{1.3}$$

$$\begin{bmatrix} \phi & P \end{bmatrix} \begin{pmatrix} c \\ d \end{pmatrix} \quad = \quad (f)$$

where the second summation (referred to as *interpolation conditions* [35]) ensures the minimum degree of the interpolant. Refer to Table 1.1 for a short list of recommended RBFs and minimally required orders of m. This document prefers the Gaussian RBF. Notice, in Equation 1.3, that the interpolation conditions add M new degrees of freedom, so we must provide M additional constraints to square the system. In this case:

$$\sum_{j=1}^{N} c_j P_l(x_j) = 0, \qquad l = 1, ..., M$$

or

$$P^T c = 0. \tag{1.4}$$

It is now possible again to write the interpolation problem as a complete linear system using Equations 1.3 and 1.4:

$$\underbrace{\begin{bmatrix} \phi & P \\ P^T & 0 \end{bmatrix}}_{A} \begin{pmatrix} c \\ d \end{pmatrix} = \begin{pmatrix} f \\ 0 \end{pmatrix} \tag{1.5}$$

Equation 1.5—typically a dense system except in the case of RBFs with compact support—can be solved efficiently via standard methods like LU-decomposition. With the coefficients, the interpolant can be sampled at any test points, $\{x_i\}_{i=1}^{n}$, by substitution into Equation 1.3:

$$f(x_i) \quad = \quad \sum_{j=1}^{N} c_j \phi_j(x_i) + \sum_{l=1}^{M} d_l P_l(x_i)$$

$$= \quad \underbrace{\begin{bmatrix} \phi & P \end{bmatrix}}_{B} \begin{pmatrix} c \\ d \end{pmatrix} \Bigg|_{x=x_i} \tag{1.6}$$

1.2.2 Reconstructing Solutions for PDEs

In the next few subsections, we will consider collocation equations based on this general form:

$$\begin{aligned} \mathcal{L} u_\phi(x) &= f(x) & \text{on } \Omega \\ \mathcal{B} u_\phi(x) &= g(x) & \text{on } \Gamma \end{aligned}$$

where the methods presented below will apply the differential operators, $\mathcal{L}$ and $\mathcal{B}$, to different choices of u_ϕ and different sets of collocation points. In many applications $\mathcal{L}$ is chosen as a differential operator (e.g., $\frac{\partial}{\partial x}$, ∇, ∇^2) and $\mathcal{B} = I$ (i.e. identity operator for Dirichlet boundary conditions) for PDEs. For RBF scattered data interpolation, $\mathcal{L} = I$. There are also applications where $\mathcal{L}$ is a convolution operator (see e.g., [5, 6]) capable of smoothing/de-noising a surface reconstructed from point clouds.

For all the methods that follow a linear system is generated:

$$A_\mathcal{L} \begin{pmatrix} c \\ d \end{pmatrix} = \begin{pmatrix} f \\ 0 \end{pmatrix}$$

$$\begin{pmatrix} c \\ d \end{pmatrix} = A_\mathcal{L}^{-1} \begin{pmatrix} f \\ 0 \end{pmatrix}$$

where matrix $A_\mathcal{L}$ depends on the choice of collocation method. Once the linear system is solved, the value $u(x)$ is reconstructed at the test points following Equation 1.6:

$$
\begin{aligned}
u(x) &\approx \begin{bmatrix} \phi & P \end{bmatrix} \begin{pmatrix} c \\ d \end{pmatrix} \Big|_{x=x_i} \\
&\approx B A_\mathcal{L}^{-1} \begin{pmatrix} f \\ 0 \end{pmatrix}
\end{aligned}
\tag{1.7}
$$

Likewise, to obtain differential quantities we have:

$$
\begin{aligned}
\mathcal{L}u(x) &\approx \begin{bmatrix} \phi_\mathcal{L} & P_\mathcal{L} \end{bmatrix} \begin{pmatrix} c \\ d \end{pmatrix} \Big|_{x=x_i} \\
&\approx B_\mathcal{L} A_\mathcal{L}^{-1} \begin{pmatrix} f \\ 0 \end{pmatrix}
\end{aligned}
$$

1.2.3   PDE Methods

Now, since $u_\phi(x)$ from Equation 1.2 cannot (in general) satisfy the PDE everywhere, we enforce the PDE at a set of collocation points, which are distributed over both the interior and the boundary. Again, these points do not necessarily coincide with the RBF centers, but it is convenient for this to be true in practice. Also, for each of the methods the choice of RBF can be either global, resulting in a large dense system, or compact, resulting in a large sparse system.

Kansa's Method

The first global RBF method for PDEs, *Kansa's method* [36, 37], collocates the solution through known values on the boundary, while constraining the interpolant to satisfy the PDE operator on the interior. This is equivalent to choosing u_ϕ according to Equation 1.2.

The resulting system is given by [43]; assuming that $\mathcal{L}$ is a linear operator,

$$\mathcal{L}u_\phi(x_i) = \sum_{j=1}^{N} c_j \mathcal{L}\phi_j(x_i) + \sum_{l=1}^{M} d_l \mathcal{L}P_l(x_i) \quad = \quad f(x_i) \quad i = 1, ..., n_I \tag{1.8}$$

$$\mathcal{B}u_\phi(x_i) = \sum_{j=1}^{N} c_j \mathcal{B}\phi_j(x_i) + \sum_{l=1}^{M} d_l \mathcal{B}P_l(x_i) \quad = \quad g(x_i) \quad i = n_I + 1, \cdots, n \tag{1.9}$$

$$\sum_{j=1}^{N} c_j P_l(x_j) \quad = \quad 0 \qquad l = 1, \cdots, M \tag{1.10}$$

where n_I are the number of interior collocation points, with the number of boundary collocation points equal to $n - n_I$. First, observe that the differential operators are applied directly to the RBFs inside summations, rather than first solving the scattered data interpolation problem and then applying the operator to the interpolant. Second, since the basis functions are known analytically, it is possible (although sometimes painful) to derive $\mathcal{L}\phi$ (refer to [15] for RBF derivative tables); the same is true for the polynomials P_l.

We can now reformulate Kansa's method as the linear system:

$$\underbrace{\begin{bmatrix} \phi_\mathcal{L} & P_\mathcal{L} \\ \phi_\mathcal{B} & P_\mathcal{B} \\ P^T & 0 \end{bmatrix}}_{A_\mathcal{L}} \begin{pmatrix} c \\ d \end{pmatrix} = \begin{pmatrix} f \\ g \\ 0 \end{pmatrix} \tag{1.11}$$

where $\phi_\mathcal{L} = \mathcal{L}\phi$, $P_\mathcal{L} = \mathcal{L}P$ are the interior components (Equation 1.8), $\phi_\mathcal{B}$ and $P_\mathcal{B}$ are the boundary components (Equation 1.9), and $P^T = \begin{bmatrix} P_\mathcal{L}^T & P_\mathcal{B}^T \end{bmatrix}$ are constraints for both interior and boundary polynomial parts (Equation 1.10). From Equation 1.11 it should be clear why Kansa's method is also known as the *Unsymmetric* collocation method.

Recall that the matrix in Equation 1.11 has no guarantee of non-singularity [14]; however, singularities are rare in practice [39].

Fasshauer's Method

Fasshauer's method [14] addresses the problem of singularity in Kansa's method by assuming the interpolation to be Hermite. That is, it requires higher differentiability of the basis functions (they must be at least C^k-continuous if $\mathcal{L}$ is of order k). Leveraging this assumption, Fasshauer's method chooses:

$$u_\phi(x_i) \quad = \quad \sum_{j=1}^{N_I} c_j \mathcal{L}\phi_j(x_i) + \sum_{j=N_I+1}^{N} c_j \mathcal{B}\phi_j(x_i) + \sum_{l=1}^{M} d_l P_l(x_i) \tag{1.12}$$

as the interpolant passing through collocation points. Note N_I is used here to specify the number of RBF centers in the interior of Ω. Here the interpolant is similar to Equation 1.2, but a change of basis functions is used for the expansion: $\mathcal{L}\phi_j(x)$ on the interior and $\mathcal{B}\phi_j(x)$ on the boundary.

Substituting Equation 1.12 into Equations 1.8-1.10 we get:

$$\sum_{j=1}^{N_I} c_j \mathcal{L}^2 \phi_j(x_i) + \sum_{j=N_I+1}^{N} c_j \mathcal{L}\mathcal{B}\phi_j(x_i) + \sum_{l=1}^{M} d_l \mathcal{L}P_l(x_i) = f(x_i) \quad i = 1,...,n_I \quad (1.13)$$

$$\sum_{j=1}^{N_I} c_j \mathcal{B}\mathcal{L}\phi_j(x_i) + \sum_{j=N_I+1}^{N} c_j \mathcal{B}^2 \phi_j(x_i) + \sum_{l=1}^{M} d_l \mathcal{B}P_l(x_i) = g(x_i) \quad i = n_I + 1,...,n$$

$$\sum_{j=1}^{N_I} c_j \mathcal{L}P_l(x_j) + \sum_{j=N_I+1}^{N} c_j \mathcal{B}P_l(x_j) = 0 \quad l = 1,...,M$$

which becomes the following:

$$\underbrace{\begin{bmatrix} \phi_{\mathcal{L}\mathcal{L}} & \phi_{\mathcal{L}\mathcal{B}} & P_{\mathcal{L}} \\ \phi_{\mathcal{B}\mathcal{L}} & \phi_{\mathcal{B}\mathcal{B}} & P_{\mathcal{B}} \\ P_{\mathcal{L}}^T & P_{\mathcal{B}}^T & 0 \end{bmatrix}}_{A_{\mathcal{L}}} \begin{pmatrix} c \\ d \end{pmatrix} = \begin{pmatrix} f \\ g \\ 0 \end{pmatrix} \quad (1.14)$$

Note that $\phi_{\mathcal{L}\mathcal{L}}$ represents the first summation in Equation 1.13.

The symmetry of Fasshauer's (*symmetric collocation*) method is apparent in Equation 1.14. Likewise, it is clear that the symmetric method requires more storage and computation to solve compared to Kansa's method. However, based on the assumption that collocation points coincide with RBF centers, the symmetry reduces storage requirements by half.

Direct Collocation

In *Direct collocation* (see [17, 39], the interpolant is chosen as Equation 1.2 (the same as Kansa's method). However, the Direct method collocates both the interior and boundary operators at the boundary points:

$$\sum_{j=1}^{N} c_j \mathcal{L}\phi_j(x_i) + \sum_{l=1}^{M} d_l \mathcal{L}P_l(x_i) = f(x_i) \quad i = 1,...,n \quad (1.15)$$

$$\sum_{j=1}^{N} c_j \mathcal{B}\phi_j(x_i) + \sum_{l=1}^{M} d_l \mathcal{B}P_l(x_i) = g(x_i) \quad i = 1,...,n_B = n - n_I$$

$$\sum_{j=1}^{N} c_j P_l(x_j) = 0 \quad l = 1,...,M$$

Reformulating as a linear system we get:

$$\begin{bmatrix} \phi_{\mathcal{L}} & P_{\mathcal{L}} \\ \phi_{\mathcal{B}} & P_{\mathcal{B}} \\ P^T & 0 \end{bmatrix} \begin{pmatrix} c \\ d \end{pmatrix} = \begin{pmatrix} f \\ g \\ 0 \end{pmatrix} \quad (1.16)$$

While the final system in Equation 1.16 is structured the same as Kansa's method (Equation 1.11), careful inspection of the index i in Equations 1.8 and 1.15 reveals that Direct collocation produces a larger system.

RBF-PS

The extension of global collocation to traditional pseudo-spectral form was introduced by Fasshauer in [13]. Dubbed RBF-PS, the method utilizes the same logic from Kansa's and Fasshauer's collocation methods to form matrix $A_\mathcal{L}$ (i.e., $A_\mathcal{L}$ can be either Equation 1.11 or 1.14). However, RBF-PS subtly assumes the solution, $u(x)$, is only required at collocation points (i.e., $\{x_i\} = \{x_c\}$) [13, 15]. Then, extending Equation 1.7, RBF-PS gives:

$$
\begin{aligned}
u(x) &= \left(B A_\mathcal{L}^{-1}\right) \begin{pmatrix} f \\ 0 \end{pmatrix} \\
&= D_\mathcal{L}^T \begin{pmatrix} f \\ 0 \end{pmatrix}.
\end{aligned}
\tag{1.17}
$$

where $D_\mathcal{L}$ is a discrete differentiation matrix (DM) for the operator $\mathcal{L}$. Here, $D_\mathcal{L}$ is independent of the function $f(x)$ and is assembled by solving the system:

$$
D_\mathcal{L} = A_\mathcal{L}^{-T} B^T
\tag{1.18}
$$

An LU-decomposition ($O(N^3)$) in preprocessing with forward- and back-solves ($O(N^2)$) are fitting to efficiently solve the multiple RHS system[15, 60].

Since matrix $D_\mathcal{L}$ is independent of functions $u(x)$ and $f(x)$, the matrix requires update only if the RBF centers move—a compelling benefit for time-dependent problems on stationary nodes. The complexity of RBF-PS for time-dependent solutions is then reduced to a matrix-vector multiply ($O(N^2)$) for each time-step. In contrast, classic RBF collocation methods also construct LU factors of $A_\mathcal{L}^{-1}$ in preprocessing, but delay application of forward- and back-solves to acquire time-dependent weighting coefficients at each time-step. This is then followed by the pre-multiply of B (i.e., additional $O(N^2)$) to complete the time-step.

1.2.4 Local Methods

Another trend in RBF methods is to use compact support to produce local linear systems defined at each collocation point. Examples of this include [55, 56] for Kansa's method, [50, 51, 52] for Fasshauer's method. To our knowledge no one has considered local Direct collocation. Also, instead of specifying a cut-off radius for RBF support, some authors specify the exact stencil size (i.e., number of neighboring points to include); see e.g., [12, 50].

After observing the general structure of the symmetric and unsymmetric collocation methods above, it is necessary only to present the symmetric (i.e. Fasshauer's) local method and note that in the unsymmetric case certain blocks will be zero allowing the system to shrink.

The formula for the interpolant local to the (k)-th collocation point (i.e., RBF center) is given by:

$$
u_\phi^{(k)}(x_i) = \sum_{j(k)=1}^{N_I} c_j^{(k)} \mathcal{L}\phi_j(x_i) + \sum_{j(k)=N_I+1}^{N_S} c_j^{(k)} \mathcal{B}\phi_j(x_i) + \sum_{l=1}^{M} d_l^{(k)} P_l(x_i)
$$

where N_S represents the number of points that defines the local stencil; N is possibly a function of the cut-off radius in the RBF, N_I is the number of interior stencil points (those

16

points of the stencil that lie in the interior of Ω). The index j is a function of the stencil center k allowing the system to include a local neighborhood of stencil points.

This results in a linear system with similar structure to the global collocation problem, but the dimensions are much smaller:

$$\underbrace{\begin{bmatrix} \phi_{\mathcal{L}\mathcal{L}} & \phi_{\mathcal{L}\mathcal{B}} & P_{\mathcal{L}} \\ \phi_{\mathcal{B}\mathcal{L}} & \phi_{\mathcal{B}\mathcal{B}} & P_{\mathcal{B}} \\ P_{\mathcal{L}}^{T} & P_{\mathcal{B}}^{T} & 0 \end{bmatrix}}_{A_{\mathcal{L}}} \begin{pmatrix} c^{(k)} \\ d^{(k)} \end{pmatrix} = \begin{pmatrix} f \\ g \\ 0 \end{pmatrix} \tag{1.19}$$

Solving this system gives an interpolant locally defined around the stencil center. Note that approximating the PDE solution $u(x)$ requires finding the stencil center nearest x, then using the local interpolant for that stencil. Since interpolation is local (i.e., $c_j^{(k)}$'s are unique to each RBF center), reconstructing the derivatives with Equation 1.8 is limited to an inner product for each center rather than the matrix-vector grouping possible with global RBFs. This approach decomposes the problem into smaller and more manageable parts. However, because the interpolants are local, there is no notion of global continuity/smoothness of the solution.

Chapter 2

Introduction to RBF-FD

While most of the literature surrounding RBFs for PDEs involves collocation, an alternative method does exist: RBF-generated Finite Differences (RBF-FD). RBF-FD is a hybrid of RBF scattered data interpolation and Finite Difference (FD) stencils.

The idea behind FD stencils is to express various derivative operators as a linear combination of known functional values in the neighborhood of a point where an approximation to the derivative operator is desired. Common approximations such as upwind differencing, center differencing, and higher order approximations are of this form. Similarly, RBF-FD combines functional values, but it does so in a more generalized sense than standard FD stencils. While one is typically restricted to regular meshes and often symmetric stencils in classic FD, RBF-FD allows for stencils with irregular placement and number of nodes.

The choice to study RBF-FD within this work is motivated by two factors. First, RBF-FD represents one of the latest developments within the RBF community. The method was first introduced in 2000 [54], but is only now showing signs it has obtained the critical-mass following necessary for the method's use in large-scale scientific models. Our goal throughout the dissertation has been to scale RBF-FD to complex problems on high resolution meshes, and to lead the way for its adoption in high performance computational geophysics. Graphics Processing Units (GPUs), introduced in Chapter ??, are many-core accelerators capable of general purpose, embarrassingly parallel computations. GPUs represent the latest trend in high performance computing, where compute nodes are commonly supplemented by one or more accessory GPUs. Our effort leads the way for application of RBF-FD in an age when compute nodes with attached accelerator boards will be key to breaching the exa-scale computing barrier [2]. Second, RBF-FD inherits many of the positive features from global and local collocation schemes, but sacrifices others for reduced computational complexity and potentially increased parallelism. The method is sufficiently young, so many opportunities for investigation still remain. Key challenges lie in the choice of grid, the choice of stencil, whether or not to change the support as a function of the stencil, how to guaranty the stability of the differentiation operator after discretization, etc.

2.1 Background

RBF-generated Finite Differences (RBF-FD) were first introduced by Tolstykh in 2000 [54], but it was the simultaneous, yet independent, efforts in [48], [53], [59] and [7] that gave the method its real start. The RBF-FD method (and the RBF-HFD, "Hermite" equivalent [61]) is similar in concept to classical finite-differences (FD), but differs in that the underlying differentiation weights are exact for RBFs rather than polynomials. The method contrasts with global RBF methods in the sense that it does not collocate the PDE. Instead, RBF-FD provides a set of generalized FD weights representing the discrete differential operator for a small neighborhood of nodes.

RBF-FD share many advantages with global RBF methods, like the ability to function without an underlying mesh, easily extend to higher dimensions and afford large time steps; however spectral accuracy is lost. Other advantages of RBF-FD include lower computational complexity together with high-order accuracy (6th to 10th order accuracy is common). As in FD, increasing the stencil size, n, increases the order accuracy of the approximation. While not a panacea for PDEs, the method is simple to code, easily extensible to higher dimensions, and powerful in its ability to avoid singularities introduced by the coordinate systems that might impact other methods (see e.g., [21, 27]).

In some ways, RBF-FD and global RBF methods are plagued by the same difficulties. For example, as the number of nodes in the stencil increases, so too does the ill-conditioning of the linear systems to be inverted. Similarly, the most accurate weights occur when $\epsilon \to 0$, but values in that regime beget additional ill-conditioning problems—a recurrence of the *Uncertainty Relation* [45]. One key difference in the multiple independent RBF-FD origins was that Wright [59] focused on bypassing ill-conditioning of RBF-FD and investigated its behavior in the limit as $\epsilon \to 0$ by means of the Contour-Padé algorithm.

Given N total nodes in the domain, N linear systems, each of size $(n+1) \times (n+1)$, are solved to calculate the differentiation weights for derivatives at each node. With $n \ll N$, the RBF-FD preprocessing complexity is dominated by $O(N)$; significantly lower than the global RBF or RBF-PS methods ($O(N^3)$). Additionally, the cost per time step is also dominated by $O(N)$.

RBF-FD have been successfully employed for a variety of problems including Hamilton-Jacobi equations [7], convection-diffusion problems [8, 50], incompressible Navier-Stokes equations [9, 48], transport on the sphere [27], and the shallow water equations [20]. Shu et al. [49] compared the RBF-FD method to Least Squares FD (LSFD) in context of 2D incompressible viscous cavity flow, and found that under similar conditions, the RBF-FD method was more accurate than LSFD, but the solution required more iterations of an iterative solver. RBF-FD was applied to Poisson's equation in [58]. Chandhini and Sanyasiraju [8] studied it in context of 1D and 2D, linear and non-linear, convection-diffusion equations, demonstrating solutions that are non-oscillatory for high Reynolds number, with improved accuracy over classical FD. An application to Hamilton-Jacobi problems [7], and 2D linear and non-linear PDEs including Navier-Stokes equations [48] have all been considered.

2.2 The RBF-generated Finite Differences Method

The RBF-FD method is similar to classical Finite Differences in that RBF-FD allows derivatives of a function $u(x)$ to be approximated by weighted combinations of n function values in a small neighborhood (i.e., $n \ll N$) around a *center* node, x_c. That is:

$$\mathcal{L}u(x) \mid_{x=x_c} \approx \sum_{j=1}^{n} c_j u(x_j) \tag{2.1}$$

where $\mathcal{L}u$ again represents a differential quantity over $u(x)$ (e.g., $\mathcal{L} = \frac{\partial}{\partial x}$). We refer to the n nodes around x_c as a *stencil* with size n. While not required, in practice one considers stencils to include the center, x_c, plus the $n-1$ nearest neighboring nodes. The definition of "nearest" depends the choice of distance metric; here, Euclidean distance ($\|x - x_c\|_2$) is preferred.

Generally, one typically needs derivatives at every node in the discretized domain to solve PDEs. To achieve this with RBF-FD, stencils are generated around each node in the domain. Stencils need not have the same size (n), but this is assumed here for simplicity in discussion. Furthermore, the number of stencils need not match the number of nodes in the domain, but this is also assumed.
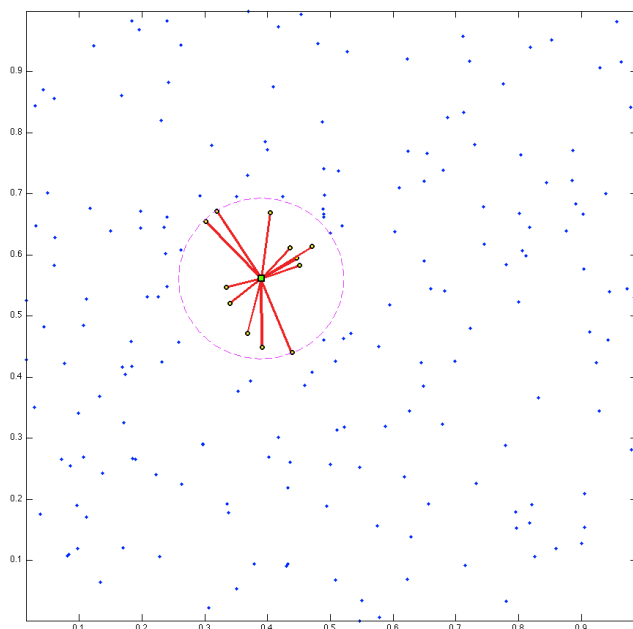
(a) A 13 node RBF-FD stencil of randomly distributed nodes. The stencil centered at the green square contains the 12 nearest neighbors contained within the minimum covering circle drawn in purple.
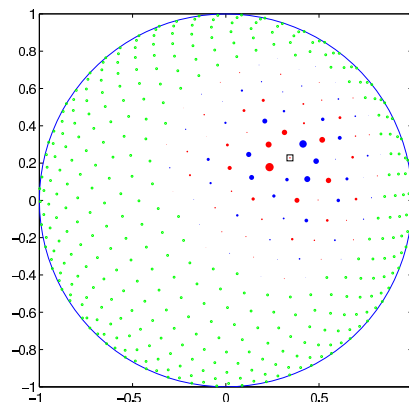
(b) A 75 node RBF-FD stencil with blue (negative) and red (positive) differentiation weights to approximate advective operator at the square. Stencils weights indicated by scale of disk radii. (Image courtesy of Bengt Fornberg and Natasha Flyer)

Figure 2.1: Examples of stencils computable with RBF-FD

Figure 2.1 provides two examples of RBF-FD stencils. First, Figure 2.1a illustrates a single stencil of size $n = 13$ in a domain of randomly distributed nodes. The stencil center,

x_c, is represented by a green square, with the 12 neighboring nodes connected via red edges. The purple circle, the minimum covering circle for the stencil, demonstrates that the stencil contains only the 12 nearest neighbors of the center node. In Figure 2.1b, a larger RBF-FD stencil of size $n = 75$ on the unit sphere is shown as red and blue disks surrounding the center represented as a square. Green disks are nodes outside of the stencil. The radii and color of the red and blue disks represent the magnitude and alternating sign of coefficients, c_j, determined to calculate a derivative quantity at the stencil center.

2.2.1   Stencil Weights

To approximate $\mathcal{L}u(x)$, one requires the stencil *weights* (coefficients), c_j. Stencil weights are a discrete representation of the differential operator at the stencil center and may vary by node location (e.g., nodes at the boundary are usually governed by another operator, $\mathcal{B}$). Weights are obtained by enforcing that they be exact within the space spanned by the RBFs centered at stencil nodes (i.e., $\phi_j(x) = \phi(\epsilon||x - x_j||_2)$; an RBF centered at x_j). Various studies [20, 23, 27, 61] show that better accuracy is achieved when the interpolant can exactly reproduce a constant, p_0, such that

$$\mathcal{L}\phi_i(x) \mid_{x=x_c} = \sum_{j=1}^{n} c_j \phi_j(x_i) + c_{n+1}p_0 \qquad \text{for } i = 1, 2, ..., n$$

with $\mathcal{L}\phi_i$ provided by analytically applying the differential operator to the RBF. Assuming $p_0 = 1$, the constraint $\sum_{i=1}^{n} c_i = \mathcal{L}p_0|_{x=x_c} = 0$ completes the system:

$$\begin{bmatrix} \phi_1(x_1) & \phi_2(x_1) & \cdots & \phi_n(x_1) & 1 \\ \phi_1(x_2) & \phi_2(x_2) & \cdots & \phi_n(x_2) & 1 \\ \vdots & \ddots & \ddots & \vdots & \vdots \\ \phi_1(x_n) & \phi_2(x_n) & \cdots & \phi_n(x_n) & 1 \\ 1 & 1 & \cdots & 1 & 0 \end{bmatrix} \begin{pmatrix} c_1 \\ c_2 \\ \vdots \\ c_n \\ c_{n+1} \end{pmatrix} = \begin{pmatrix} \mathcal{L}\phi_1(x) \mid_{x=x_c} \\ \mathcal{L}\phi_2(x) \mid_{x=x_c} \\ \vdots \\ \mathcal{L}\phi_n(x) \mid_{x=x_c} \\ 0 \end{pmatrix} \qquad (2.2)$$

$$\begin{bmatrix} \phi & P \\ P^T & 0 \end{bmatrix} \begin{pmatrix} c_{\mathcal{L}} \\ d_{\mathcal{L}} \end{pmatrix} = \begin{pmatrix} \phi_{\mathcal{L}} \\ 0 \end{pmatrix}.$$

The choice of $\mathcal{L}$ can be any linear operator. As an example, if $\mathcal{L}$ is the identity operator, then the above procedure leads to RBF-FD weights for interpolation. If $\mathcal{L} = \frac{\partial}{\partial x}$, one obtains the weights to approximate the first derivative in x. Refer to [15] for a table of commonly used RBF derivatives. Section 2.3 provides a list of derivatives used in this work.

The small $(n + 1) \times (n + 1)$ system in Equation 2.2 is dense, and is solved at a cost of $O(n^3)$ floating point operations (FLOPs) using direct methods like LU-decomposition. The resulting stencil weights, $c_{\mathcal{L}} = \{c_j\}_{j=1}^{n}$ can be substituted into Equation 2.1 for the derivative approximation at x_c. Coefficient c_{n+1} ($d_{\mathcal{L}} = c_{n+1}$), included in the solution of Equation 2.2, is of no use and discarded once the system has been solved.

Based on the choice of support parameter, ϵ, the Equation 2.2 may suffer problems with conditioning. In such cases, stable methods like Contour–Padé [59] or RBF-QR [11, 26] may be preferred.

2.2.2 Differentiation Matrix

Note that Equation 2.2 resolves the weights only for the stencil x_c. The small system solve is repeated N times—once for each stencil—to obtain a total of $N \times n$ stencil weights.

For PDEs, it is common practice to assemble a *differentiation matrix* (DM); a discrete representation of the PDE operator on the domain. Given the set of nodes in the domain $\{x_k\}_{k=1}^N$, the c-th row of the DM represents the discrete PDE operator for the stencil centered at node x_c with stencil nodes $\{x_j\}_{j=1}^n$:

$$\mathcal{L}u(x) \approx D_{\mathcal{L}}u$$

$$D_{\mathcal{L}}^{(c,k)} = \begin{cases} c_j & x_k = x_j \\ 0 & x_k \neq x_j \end{cases}$$

where (c, k) represents the (row, column) index of $D_{\mathcal{L}}$ and vector $u = \{u(x_k)\}_{k=1}^N$. Equation 2.1 can be rewritten as:

$$\mathcal{L}u(x)\mid_{x=x_c} \approx D_{\mathcal{L}}^{(c)}u \quad .$$

In the solution of PDEs the DMs are utilized in explicit and implicit modes. Here explicit implies evaluating the matrix-vector mulitply to get derivative values, u', from explicitly known vector of solution values u:

$$u' = D_{\mathcal{L}}u$$

whereas implicit solves for unknown u:

$$D_{\mathcal{L}}u = f$$

An example RBF-FD DM is illustrated in Figure 2.2. In this example, assume operator $\mathcal{L} = \frac{\partial}{\partial x}$ is approximated at all N stencil centers of an arbitrary domain. RBF-FD weights assemble the rows of the differentiation matrix, D_x. On each row, weights are indicated by blue dots. The sparsity of rows reflects the subset of $\{x_k\}_{k=1}^N$ included in corresponding stencils of size n. On the right hand side, discrete derivative values $\frac{du}{dx}$ are approximated at all stencil centers.

Differentiation matrices are assembled at a cost of $O(n^3N)$ FLOPs. However, since the goal of RBF-FD is to keep stencil neighborhoods small ($n \ll N$), the cost of assembly scales as $O(N)$. Furthermore, RBF-FD weights are independent of function values ($u(x)$) and rely only on stencil node locations. The implications of this are as profound as in the context RBF-PS for time-dependent PDEs: the stencil weights are constant so long as the nodes are stationary. Thus, the DM assembly is part of a one-time preprocessing step.

The sparsity exhibited by the DM in Figure 2.2 is typical for RBF-FD due to $n \ll N$. Best practices dictate that the DMs be stored in a compressed sparse storage format to retain only non-zeros and their corresponding indices in memory.

2.2.3 Multiple Operators

In many cases, multiple derivatives (e.g., $\mathcal{L} = \nabla^2$, $\frac{\partial}{\partial x}$, $\frac{\partial}{\partial y}$, etc.) are required at stencil centers. This is common, for example, when solving coupled PDEs. For RBF-FD, acquiring
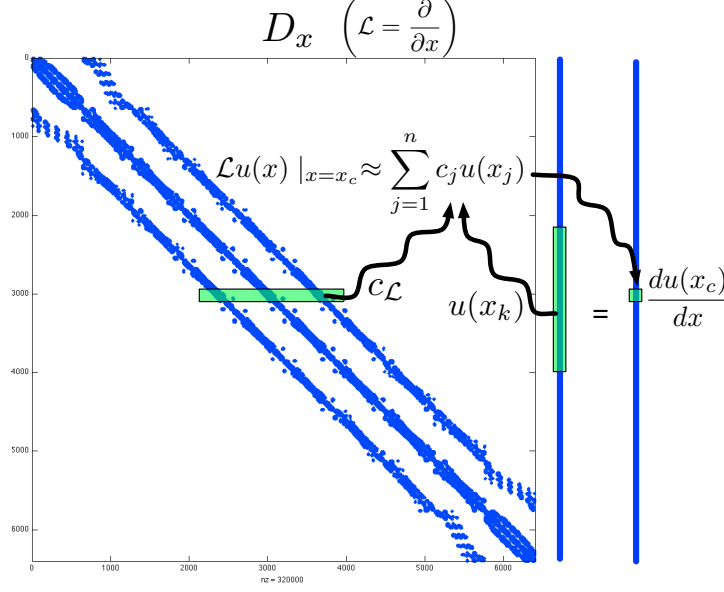
Figure 2.2: Differentiation matrix D_x is applied to the solution values $u(x)$ to obtain derivative approximations, $\frac{du}{dx}$.

weights for each additional operator can be both straight-forward and computationally efficient. For each change of differential operator, observe that only the RHS of Equation 2.2 is modified. Thus, new operators amount to extending Equation 2.2 to solve

$$
\begin{bmatrix} \phi & P \\ P^T & 0 \end{bmatrix} \begin{bmatrix} c_{\nabla^2} & c_x & c_y & \cdots \\ d_{\nabla^2} & d_x & d_y & \cdots \end{bmatrix} = \begin{bmatrix} \phi_{\nabla^2} & \phi_x & \phi_y & \cdots \\ 0 & 0 & 0 & \cdots \end{bmatrix}.
$$

where multiple sets of weights (c_∇, c_x, c_y) solved simultaneously. This dense, symmetric, multiple RHS linear system is considered ideal by linear algebra packages, and many highly optimized routines exist to solve them (e.g., LAPACK "dgesv") [1].

2.3 Weight Operators

In the course of this work we work with a variety of PDEs. This section enumerates a list of relevant operators and their corresponding equations for the RHS of Equation 2.2. Whenever possible the general form of $\mathcal{L}\phi$ is provided; otherwise the Gaussian RBF ($\phi(r) = e^{-(\epsilon r)^2}$) is assumed.

2.3.1 First and Second Derivatives ($\frac{1}{r}\frac{\partial \phi}{\partial r}, \frac{\partial^2 \phi}{\partial r^2}$)

The following are used in subsequent derviatives:

$$
\frac{1}{r}\frac{d}{dr}\phi(r) = -2\epsilon^2 \phi(r)
$$

$$
\frac{\partial^2 \phi}{\partial r^2} = \epsilon^2(-2 + 4(\epsilon r)^2)\phi(r)
$$

2.3.2 Cartesian Gradient (∇)

The first derivatives in Cartesian coordinates $(\frac{\partial}{\partial x}, \frac{\partial}{\partial y}, \frac{\partial}{\partial z})$ are produced via the chain rule:

$$\frac{\partial \phi}{\partial x} = \frac{\partial r}{\partial x}\frac{\partial \phi}{\partial r} = \frac{(x - x_j)}{r}\frac{\partial \phi}{\partial r}$$

$$\frac{\partial \phi}{\partial y} = \frac{\partial r}{\partial y}\frac{\partial \phi}{\partial r} = \frac{(y - y_j)}{r}\frac{\partial \phi}{\partial r}$$

$$\frac{\partial \phi}{\partial z} = \frac{\partial r}{\partial z}\frac{\partial \phi}{\partial r} = \frac{(z - z_j)}{r}\frac{\partial \phi}{\partial r}$$

where $\frac{\partial \phi}{\partial r}$ for the Gaussian RBFs is given above.

2.3.3 Cartesian Laplacian (∇^2)

Fasshauer [15] provides the general form of ∇^2 in 2D as:

$$\nabla^2 = \frac{\partial^2}{\partial r^2}\phi(r) + \frac{1}{r}\frac{\partial}{\partial r}\phi(r)$$

For Gaussian RBFs in particular we have the following operators:

- 1D:
$$\nabla^2 = \epsilon^2(-2 + 4(\epsilon r)^2)\phi(r)$$

- 2D:
$$\nabla^2 = \epsilon^2(-4 + 4(\epsilon r)^2)\phi(r)$$

- 3D:
$$\nabla^2 = \epsilon^2(-6 + 4(\epsilon r)^2)\phi(r)$$

which all fit $\nabla^2 = \frac{\partial^2}{\partial r^2}\phi(r) + \frac{d-1}{r}\frac{\partial}{\partial r}\phi(r)$ for dimension d.

2.3.4 Laplace-Beltrami (Δ_S) on the Sphere

The ∇^2 operator can be represented in spherical polar coordinates for $\mathbb{R}^3$ as:

$$\nabla^2 = \underbrace{\frac{1}{r}\frac{\partial}{\partial r}\left(r^2\frac{\partial}{\partial r}\right)}_{\text{radial}} + \underbrace{\frac{1}{r^2}\Delta_S}_{\text{angular}},$$

where Δ_S is the Laplace-Beltrami operator—i.e., the Laplacian operator constrained to the surface of the sphere. This form nicely illustrates the separation of components into radial and angular terms.

In the case of PDEs solved on the unit sphere, there is no radial term, so we have:

$$\nabla^2 \equiv \Delta_S. \tag{2.3}$$

Although this originated in the spherical coordinate system, [60] introduced the following Laplace-Beltrami operator for the surface of the sphere:

$$\Delta_S = \frac{1}{4}\left[\left(4-r^2\right)\frac{\partial^2\phi}{\partial r^2} + \frac{4-3r^2}{r}\frac{\partial\phi}{\partial r}\right],$$

where r is the Euclidean distance between nodes of an RBF-FD stencil and is independent of our choice of coordinate system.

2.3.5 Constrained Gradient ($P_x \cdot \boldsymbol{\nabla}$) on the Sphere

Following [20, 22], the gradient operator can be constrained to the sphere with this projection matrix:

$$P = I - \mathbf{x}\mathbf{x}^T = \begin{pmatrix} (1-x_1^2) & -x_1x_2 & -x_1x_3 \\ -x_1x_2 & (1-x_2^2) & -x_2x_3 \\ -x_1x_3 & -x_2x_3 & (1-x_3^2) \end{pmatrix} = \begin{pmatrix} P_{x_1} \\ P_{x_2} \\ P_{x_3} \end{pmatrix} \tag{2.4}$$

where $\mathbf{x}$ is the unit normal at the stencil center.

The direct method of computing RBF-FD weights for the projected gradient for $\mathbf{P}\cdot\nabla$ is presented in [22]. When solving for the weights, we apply the projection on the right hand side of our small linear system. We let $\mathbf{x} = (x_1, x_2, x_3)$ be the stencil center, and $\mathbf{x}_k = (x_{1,k}, x_{2,k}, x_{3,k})$ indicate an RBF-FD stencil node.

Using the chain rule, and assumption that

$$r(\mathbf{x}_k - \mathbf{x}) = ||\mathbf{x}_k - \mathbf{x}|| = \sqrt{(x_{1,k} - x_1)^2 + (x_{2,k} - x_2)^2 + (x_{3,k} - x_3)^2},$$

we obtain the unprojected gradient of ϕ as

$$\nabla\phi(r(\mathbf{x}_k - \mathbf{x})) = \frac{\partial r}{\partial \mathbf{x}}\frac{\partial\phi(r(\mathbf{x}_k - \mathbf{x}))}{\partial r} = -(\mathbf{x}_k - \mathbf{x})\frac{1}{r(\mathbf{x}_k - \mathbf{x})}\frac{\partial\phi(r(\mathbf{x}_k - \mathbf{x}))}{\partial r}.$$

Applying the projection matrix gives

$$\mathbf{P}\nabla\phi(r(\mathbf{x}_k - \mathbf{x})) = -(\mathbf{P}\cdot\mathbf{x}_k - \mathbf{P}\cdot\mathbf{x})\frac{1}{r(\mathbf{x}_k - \mathbf{x})}\frac{\partial\phi(r(\mathbf{x}_k - \mathbf{x}))}{\partial r}$$

$$= -(\mathbf{P}\cdot\mathbf{x}_k - 0)\frac{1}{r(\mathbf{x}_k - \mathbf{x})}\frac{\partial\phi(r(\mathbf{x}_k - \mathbf{x}))}{\partial r}$$

$$= -(I - \mathbf{x}\mathbf{x}^T)(\mathbf{x}_k)\frac{1}{r(\mathbf{x}_k - \mathbf{x})}\frac{\partial\phi(r(\mathbf{x}_k - \mathbf{x}))}{\partial r}$$

$$= \begin{pmatrix} x\mathbf{x}^T\mathbf{x}_k - x_k \\ y\mathbf{x}^T\mathbf{x}_k - y_k \\ z\mathbf{x}^T\mathbf{x}_k - z_k \end{pmatrix}\frac{1}{r(\mathbf{x}_k - \mathbf{x})}\frac{\partial\phi(r(\mathbf{x}_k - \mathbf{x}))}{\partial r}$$

Thus, we directly compute the weights for $P_x \cdot \boldsymbol{\nabla}$ using these three RHS in Equation 2.2:

$$P\frac{\partial}{\partial x_1} = (x_1\mathbf{x}^T\mathbf{x}_k - x_{1,k})\frac{1}{r(\mathbf{x}_k - \mathbf{x})}\frac{\partial\phi(r(\mathbf{x}_k - \mathbf{x}))}{\partial r}\Big|_{\mathbf{x}=\mathbf{x}_j}$$

$$P\frac{\partial}{\partial x_2} = (x_2\mathbf{x}^T\mathbf{x}_k - x_{2,k})\frac{1}{r(\mathbf{x}_k - \mathbf{x})}\frac{\partial\phi(r(\mathbf{x}_k - \mathbf{x}))}{\partial r}\Big|_{\mathbf{x}=\mathbf{x}_j}$$

$$P\frac{\partial}{\partial x_3} = (x_3\mathbf{x}^T\mathbf{x}_k - x_{3,k})\frac{1}{r(\mathbf{x}_k - \mathbf{x})}\frac{\partial\phi(r(\mathbf{x}_k - \mathbf{x}))}{\partial r}\Big|_{\mathbf{x}=\mathbf{x}_j}$$

2.3.6 Hyperviscosity Δ^k for Stabilization

When explicitly solving hyperbolic equations, differentiation matrices encode convective operators of the form

$$D = \alpha \frac{\partial}{\partial \lambda} + \beta \frac{\partial}{\partial \theta} \tag{2.5}$$

The convective operator, discretized through RBF-FD, has eigenvalues in the right half-plane causing the method to be unstable [20, 27]. Stabilization of the RBF-FD method is achieved through the application of a hyperviscosity filter to Equation (2.5) [27]. By using Gaussian RBFs, $\phi(r) = e^{-(\epsilon r)^2}$, the hyperviscosity (a high order Laplacian operator) simplifies to

$$\Delta^k \phi(r) = \epsilon^{2k} p_k(r) \phi(r) \tag{2.6}$$

where k is the order of the Laplacian and $p_k(r)$ are multiples of generalized Laguerre polynomials that are generated recursively ([27]):

$$\begin{cases} p_0(r) & = 1, \\ p_1(r) & = 4(\epsilon r)^2 - 2d, \\ p_k(r) & = 4((\epsilon r)^2 - 2(k-1) - \frac{d}{2})p_{k-1}(r) - 8(k-1)(2(k-1) - 2 + d)p_{k-2}(r), \quad k = 2, 3, ... \end{cases}$$

where d is the dimension of the problem. In application of hyperviscosity, we assume a $d = 2$ on the surface of the sphere since individual RBF-FD stencils can be viewed as (nearly) lying on a plane. For small N, the diameter of the stencil may not be sufficiently small compared to the radius of the sphere, and hyperviscosity might not work as advertised.

In the case of parabolic and hyperbolic PDEs, hyperviscosity is added as a filter to the right hand side of the evaluation. For example, at the continuous level, the equation solved takes the form

$$\frac{\partial u}{\partial t} = -\mathcal{L}u + Hu, \tag{2.7}$$

where $\mathcal{L}$ is the PDE operator, and H is the hyperviscosity filter operator. Applying hyperviscosity shifts all the eigenvalues of L (the discrete form of $\mathcal{L}$) to the left half of the complex plane. This shift is controlled by k, the order of the Laplacian, and a scaling parameter γ_c, defined by

$$H = \gamma \Delta^k = \gamma_c N^{-k} \Delta^k.$$

It was found in [20], and verified in our own application, that $\gamma = \gamma_c N^{-k}$ provides stability and good accuracy for all values of N considered here. It also ensures that the viscosity vanishes as $N \to \infty$ [20]. In general, the larger the stencil size, the higher the order of the Laplacian. This is attributed to the fact that, for convective operators, larger stencils treat a wider range of modes accurately. As a result, the hyperviscosity operator should preserve as much of that range as possible. The parameter γ_c must also be chosen with care and its sign depends on k (for k even, γ_c will be negative and for k odd, it will be positive). If γ_c is too large, the eigenvalues move outside the stability domain of our time-stepping scheme and/or eigenvalues corresponding to lower physical modes are not left intact, reducing the accuracy of our approximation. If γ_c is too small, eigenvalues remain in the right half-plane [20, 27].

2.4 Implementation

This section details many of the steps we have taken in our practical implementation of RBF-FD. First, the method is not infallible; it faces similar conditioning issues as global/compact RBF method in that the success of the method depends on the choice of support parameter, ϵ. Second, proper choice of ϵ varies based on the underlying node distribution, as well as the generated stencils. Third, the complexity of the method is low, but there are a few

2.4.1 On Choosing the Right ϵ

If solving for the weights directly (i.e., inverting Equation 2.2), one must carefully choose ϵ to prevent ill-conditioning. Numerous attempts exist in literature to provide "good" functions for ϵ based on node spacing, h, stencil size n, etc. In general, the values provided are particular to the specific problem and/or grid under consideration. No fool-proof method exists to select the support parameters, so the prospect of hassle-free application of the RBF-FD method is still out of reach.

Modern algorithms introduced in the last couple years provide methods for acquiring weights. Contour-Padé, RBF-QR, and RBF-GA are all options for weights corresponding to the $\epsilon \to 0$. These methods appear to resolve many issues including conditioning of implicit systems for more accurate solutions [11] [?]

In this work, we have attempted a variety of scalings on ϵ. We forego discussion of these attempts since they are outside our current scope of investigation. In the end, we find that the most effective method for choosing ϵ was to adopt the approach introduced in [20], wherein ϵ is expressed as a function of the number of nodes N and desired mean condition number, $\bar{\kappa}_A$.

The optimal ϵ for general node distributions is out of the scope of this research and not necessary for our purposes. For now we assume that nodes are more or less regularly distributed, either via some algorithm such as Lloyd's method to create Centroidal Voronoi Tessellations, repelling springs (distmesh), minimum energy or minimum determinant, or some other algorithm. Except in cases where convergence on PDE solutions can not be attained via RBF-FD, we find that a direct solve for RBF-FD weights is sufficient. To a certain extent, this work considers parallelization of the method so it does not matter if our weights are precise or not.

2.4.2 Generating Stencils

For each of the N small system solves of Equation (2.2), the n nearest neighbors to $\mathbf{x}_j$ need to be located. This can be done efficiently using neighbor query algorithms or spatial partitioning data-structures such as Locality Sensitive Hashing (LSH) and kD-Tree. Different query algorithms often have a profound impact on the DM structure and memory access patterns. We choose a Raster (ijk) ordering LSH algorithm [?] leading to the matrix structure in Figures ?? and ??. While querying neighbors for each stencil is an embarrassingly parallel operation, the node sets used here are stationary and require stencil generation only once. Efficiency and parallelism for this task has little impact on the overall run-time of tests, which is dominated by the time-stepping. We preprocess node sets and generate stencils serially, then load stencils and nodes from disk at run-time. In contrast

to the RBF-FD view of a static grid, Lagrangian/particle based PDE algorithms promote efficient parallel variants of LSH in order to accelerate querying neighbors at each time-step [31, 44].

Many algorithms exist to query the k-nearest neighbors (equivalently all nodes in the minimum/smallest enclosing circle). Some algorithms overlay a grid similar to Locality Sensitive Hashing and query such as... [**?**].

RBF-FD is designed to handle irregular node distributions. Therefore, it is not essential that stencils contain only nearest neighbors. Instead, one can acquire the *approximate nearest neighbors*. Figure **??** demonstrates a case where a does not contain all nearest neighbors. As illustrated in the Figure, the ANN stencil and true nearest neighbor stencil differ by one node. THis is not dire

KDTree

Hashing

Hashing, shown in Figure **??** overlays a regular grid. This is equivalent to an axis aligned bounding box AABB, with refinement. In other words, we form a quad-tree in 2D, an octree in 3D. The neighbor query starts with the cell in which x_c resides. Since we use an axis aligned bounding box, this cell index is easily calculated given the coordinate and number of subdivisions in each dimension. Once the cell index is resolved, the stencil is populated by taking the n nearest neighbors from within the current cell. If the cell does not contain sufficient number of nodes to fill the stencil, the search for neighbors expands to include the cells immediately adjoining the center cell, taking only the nearest nodes in the provided cells. The search continues to expand outward in a rasterized circle/sphere until n is satisifed. This search is considered approximate because it can happen that a true nearest neighbor would lie in a cell that is is not included in the rasterized circle, and other nodes are substituted from the far reaches of the discretized grid.

The complexity of the method is still higher than the more efficient implementations used by Lagrangian methods, but as demonstrated in Figure **??** the savings are significant. Generating stencils for RBF-FD is a preprocessing cost, so we do not dedicate an excessive amount of attention to this algorithm. However, a few ideas that would improve: hilbert ordering, choose AABB resolution based on N not user parameters, faster sorting, GPU implementation

Savings

To demonstrate the savings in choice of stencil generation method, we provide Figure **??**.

2.4.3 Node Placement – Centroidal Voronoi Tessellation

We make the assumption for now that we use regularly distributed nodes. Centroidal Voronoi tessellations provide reasonably good distributions for solutions. Examples (heat ellipse, ellipsoid, sphere, square cavity).

The motivation behind RBF-FD is generality/functionality in the numerical method. Scattered nodes are supported. Distribution requires proper choice of support, and tight nodes result in increased conditioning

2.4.4   Approximate Nearest Neighbor (ANN) Query

RBF-FD operates on general node distributions. Historically, stencils are uniform in size (n) and generated by selecting the ($n - 1$) true nearest neighbors to a node x_c. This is a k-NN query.

Alternative queries are possible: ball query and approximate nearest neighbor. The approximate is of particular interest because nodes closest to the stencil will always be selected, whereas the nodes further away have minimal influence so swapping out cant hurt. The justification in altering the selection is for reduced complexity in neighbor queries.

For example, in general brute force is inefficient The author of [15] queries n nearest neighbors for a compact-support RBF partition of unity example with a k-D tree. In [20, 27] a k-D Tree is leveraged for all neighbor queries for RBF-FD.

In our work in [4] an alternative to k-D tree was leveraged, based loosely on Locality Sensitive Hashing.

Rather than iterate through all N nodes to find the true neighbors, or step through a k-D tree in something like $O(logN)$ that requires extra built-out, ANN allows us to use a set of nodes that satisfy

k-D Tree

Most of the RBF community leverages the k-D tree, due to its low computational complexity for querying neighbors and its wide availability as standalone software in the public domain (e.g., matlab central has a few implementations for download, and the MATLAB Statistics Toolbox includes an efficient k-D Tree).

The complexity of assembling he tree is

The Matlab central k-D Tree is MEX compiled and efficient. We integrated the standalone C++ code into our library.

While the k-D Tree functions well for queries, its downfall is a large cost in preprocessing to build the tree. For moving nodes, such as in Lagrangian schemes, this cost is prohibitively high. In an attempt to reduce the cost, lagrangian schemes introduced approximate nearest neighbor queries based on

Approximate nearest neighbors will be nearly balanced. We observe that RBF-FD functions as well on stencils of true nearest neighbors as it does on approximate nearest neighbors.

Sparsity

To quantify the sparsity of a Differentiation Matrix we consider the ratio of non-zeros ($N * n$) to total elements in the matrix (N^2). For example, a problem of size $N = 10,000$ with stencil size $n = 31$ has a ratio of 0.0031 and is 99.69% empty.

Chapter 3

A Distributed Multi-GPU RBF-FD Implementation

Parallel implementations of RBF methods currently rely on parallel domain decomposition. Depending on the implementation, domain decomposition not only accelerates solution procedures, but can decrease the ill-conditioning that plague all global RBF methods [12]. The ill-conditioning is reduced if each domain is treated as a separate RBF domain, and the boundary update is treated separately. Domain decomposition methods for RBFs were introduced by Beatson et al. [3] in the year 2000 as a way to increase problem sizes into the millions of nodes.

Divo and Kassab [12] used a domain decomposition method with artificial subdomain boundaries for their implementation of a local collocation method [12]. Subdomains are processed independently. The derivative values at artificial boundary points are averaged to maintain global consistency of physical values. Their implementation was designed for a 36 node cluster, but benchmarks and scalability tests are not provided.

Kosec and Šarler [38] used OpenMP to parallelize coupled heat transfer and fluid flow problems on a single workstation. Their test cases used local collocation, explicit time-stepping and Neumann boundary conditions. A speedup factor of 1.85x over serial execution was achieved by executing on two CPU cores; no results from scaling tests were provided.

Stevens et al. [52] mention a parallel implementation under development, but no document is available yet.

Additional RBF implementations are discussed at the end of this chapter in the context of parallel co-processing with the GPU.

In this work, we will add to the above experiences, with the added twist of incorporating an implementation on the GPU (see later chapters).

RBFs on GPU work: [46, 47] (global), [64] (compact)

Bibliography

[1] E. Anderson, Z. Bai, C. Bischof, S. Blackford, J. Demmel, J. Dongarra, J. Du Croz, A. Greenbaum, S. Hammarling, A. McKenney, and D. Sorensen. *LAPACK Users' Guide*. Society for Industrial and Applied Mathematics, Philadelphia, PA, third edition, 1999. 23

[2] Sylvie Barak. Gpu technology key to exascale says nvidia. http://www.eetimes.com/electronics-news/4230659/GPU-technology-key-to-exascale-says-Nvidia, November 2011. 18

[3] R. K. Beatson, W. A. Light, and S. Billings. Fast Solution of the Radial Basis Function Interpolation Equations: Domain Decomposition Methods. *SIAM J. Sci. Comput.*, 22(5):1717–1740, 2000. 30

[4] Evan F. Bollig, Natasha Flyer, and Gordon Erlebacher. Solution to pdes using radial basis function finite-differences (rbf-fd) on multiple gpus. *Journal of Computational Physics*, (0):–, 2012. 29

[5] J. C. Carr, R. K. Beatson, J. B. Cherrie, T. J. Mitchell, W. R. Fright, B. C. McCallum, and T. R. Evans. Reconstruction and Representation of 3D Objects with Radial Basis Functions. In *SIGGRAPH '01: Proceedings of the 28th annual conference on Computer graphics and interactive techniques*, pages 67–76, New York, NY, USA, 2001. ACM. 13

[6] J. C. Carr, R. K. Beatson, B. C. McCallum, W. R. Fright, T. J. McLennan, and T. J. Mitchell. Smooth Surface Reconstruction from Noisy Range Data. In *GRAPHITE '03: Proceedings of the 1st international conference on Computer graphics and interactive techniques in Australasia and South East Asia*, pages 119–ff, New York, NY, USA, 2003. ACM. 13

[7] Tom Cecil, Jianliang Qian, and Stanley Osher. Numerical Methods for High Dimensional Hamilton-Jacobi Equations Using Radial Basis Functions. *JOURNAL OF COMPUTATIONAL PHYSICS*, 196:327–347, 2004. 9, 19

[8] G Chandhini and Y Sanyasiraju. Local RBF-FD Solutions for Steady Convection-Diffusion Problems. *International Journal for Numerical Methods in Engineering*, 72(3), 2007. 9, 19

[9] P P Chinchapatnam, K Djidjeli, P B Nair, and M Tan. A compact RBF-FD based meshless method for the incompressible Navier–Stokes equations. *Proceedings of the*

Institution of Mechanical Engineers, Part M: Journal of Engineering for the Maritime Environment, 223(3):275–290, March 2009. 19

[10] CD Correa, D Silver, and M Chen. Volume Deformation via Scattered Data Interpolation. *Proceedings of Eurographics/IEEE VGTC Workshop on Volume Graphics*, pages 91–98, 2007. 9

[11] Oleg Davydov and Dang Thi Oanh. On the optimal shape parameter for gaussian radial basis function finite difference approximation of the poisson equation. *Computers Mathematics with Applications*, 62(5):2143 – 2161, 2011. 9, 21, 27

[12] E Divo and AJ Kassab. An Efficient Localized Radial Basis Function Meshless Method for Fluid Flow and Conjugate Heat Transfer. *Journal of Heat Transfer*, 129:124, 2007. 9, 16, 30

[13] G. E. Fasshauer. RBF Collocation Methods and Pseudospectral Methods. Technical report, 2006. 4, 7, 9, 16

[14] Gregory E. Fasshauer. Solving Partial Differential Equations by Collocation with Radial Basis Functions. In *In: Surface Fitting and Multiresolution Methods A. Le M'ehaut'e, C. Rabut and L.L. Schumaker (eds.), Vanderbilt*, pages 131–138. University Press, 1997. 6, 7, 9, 14

[15] Gregory E. Fasshauer. *Meshfree Approximation Methods with MATLAB*, volume 6 of *Interdisciplinary Mathematical Sciences*. World Scientific Publishing Co. Pte. Ltd., 5 Toh Tuck Link, Singapore 596224, 2007. 4, 5, 7, 8, 9, 11, 14, 16, 21, 24, 29

[16] Gregory E. Fasshauer and Jack G. Zhang. On choosing "optimal" shape parameters for rbf approximation. *Numerical Algorithms*, 45(1-4):345–368, 2007. 8

[17] A. I. Fedoseyev, M. J. Friedman, and E. J. Kansa. Improved Multiquadric Method for Elliptic Partial Differential Equations via PDE Collocation on the Boundary. *Computers & Mathematics with Applications*, 43(3-5):439 – 455, 2002. 6, 7, 9, 15

[18] Natasha Flyer and Bengt Fornberg. Radial basis functions: Developments and applications to planetary scale flows. *Computers & Fluids*, 46(1):23–32, July 2011. 3, 8, 9

[19] Natasha Flyer and Erik Lehto. Rotational transport on a sphere: Local node refinement with radial basis functions. *Journal of Computational Physics*, 229(6):1954–1969, March 2010. 3, 9

[20] Natasha Flyer, Erik Lehto, Sebastien Blaise, Grady B. Wright, and Amik St-Cyr. Rbf-generated finite differences for nonlinear transport on a sphere: shallow water simulations. *Submitted to Elsevier*, pages 1–29, 2011. 9, 19, 21, 25, 26, 27, 29

[21] Natasha Flyer and Grady B. Wright. Transport schemes on a sphere using radial basis functions. *Journal of Computational Physics*, 226(1):1059 – 1084, 2007. 3, 8, 9, 19

[22] Natasha Flyer and Grady B. Wright. A Radial Basis Function Method for the Shallow Water Equations on a Sphere. In *Proc. R. Soc. A*, volume 465, pages 1949–1976, December 2009. 3, 8, 9, 25

[23] B Fornberg, T Driscoll, G Wright, and R Charles. Observations on the behavior of radial basis function approximations near boundaries. *Computers & Mathematics with Applications*, 43(3-5):473–490, February 2002. 21

[24] B. Fornberg and G. Wright. Stable computation of multiquadric interpolants for all values of the shape parameter. *Computers & Mathematics with Applications*, 48(5-6):853 – 867, 2004. 4, 9, 10

[25] Bengt Fornberg, Elisabeth Larsson, and Natasha Flyer. Stable Computations with Gaussian Radial Basis Functions in 2-D. Technical Report 2009-020, Uppsala University, August 2009. 10

[26] Bengt Fornberg, Elisabeth Larsson, and Natasha Flyer. Stable Computations with Gaussian Radial Basis Functions. *SIAM J. on Scientific Computing*, 33(2):869—-892, 2011. 4, 9, 21

[27] Bengt Fornberg and Erik Lehto. Stabilization of RBF-generated finite difference methods for convective PDEs. *Journal of Computational Physics*, 230(6):2270–2285, March 2011. 9, 19, 21, 26, 29

[28] Bengt Fornberg and Cécile Piret. A Stable Algorithm for Flat Radial Basis Functions on a Sphere. *SIAM Journal on Scientific Computing*, 30(1):60–80, 2007. 4, 10

[29] Bengt Fornberg and Cécile Piret. On Choosing a Radial Basis Function and a Shape Parameter when Solving a Convective PDE on a Sphere. *Journal of Computational Physics*, 227(5):2758 – 2780, 2008. 4, 5, 9

[30] Richard Franke. Scattered Data Interpolation: Tests of Some Method. *Mathematics of Computation*, 38(157):181–200, 1982. 4, 9

[31] Prashant Goswami, Philipp Schlegel, Barbara Solenthaler, and Renato Pajarola. Interactive sph simulation and rendering on the gpu. In *Proceedings of the 2010 ACM SIGGRAPH/Eurographics Symposium on Computer Animation*, SCA '10, pages 55–64, Aire-la-Ville, Switzerland, Switzerland, 2010. Eurographics Association. 28

[32] R Hardy. Multiquadratic Equations of Topography and Other Irregular Surfaces. *J. Geophysical Research*, (76):1–905, 1971. 3, 4

[33] Y. C. Hon and R. Schaback. On unsymmetric collocation by radial basis functions. *Appl. Math. Comput.*, 119(2-3):177–186, 2001. 7, 9, 11

[34] Yiu-Chung Hon, Kwok Fai Cheung, Xian-Zhong Mao, and Edward J. Kansa. A Multiquadric Solution for the Shallow Water Equations. *ASCE J. Hydraulic Engineering*, 125:524–533, 1999. 8, 9

[35] A. Iske. *Multiresolution Methods in Scattered Data Modeling*. Springer, 2004. 4, 9, 11, 12

[36] E J Kansa. Multiquadrics–A scattered data approximation scheme with applications to computational fluid-dynamics. I. Surface approximations and partial derivative estimates. *Computers Math. Applic*, (19):127–145, 1990. 3, 5, 6, 7, 9, 13

[37] E J Kansa. Multiquadrics–A scattered data approximation scheme with applications to computational fluid-dynamics. II. Solutions to parabolic, hyperbolic and elliptic partial differential equations. *Computers Math. Applic*, (19):147–161, 1990. 3, 5, 6, 7, 9, 13

[38] G Kosec and B Šarler. Solution of thermo-fluid problems by collocation with local pressure correction. *International Journal of Numerical Methods for Heat & Fluid Flow*, 18, 2008. 9, 30

[39] Elisabeth Larsson and Bengt Fornberg. A Numerical Study of some Radial Basis Function based Solution Methods for Elliptic PDEs. *Comput. Math. Appl*, 46:891–902, 2003. 4, 7, 9, 10, 14, 15

[40] Yuxu Lin, Chun Chen, Mingli Song, and Zicheng Liu. Dual-RBF based surface reconstruction. *Vis Comput*, 25(5-7):599–607, May 2009. 9

[41] X. Liu, G.R. Liu, K. Tai, and K.Y. Lam. Radial point interpolation collocation method (RPICM) for partial differential equations. *Computers & Mathematics with Applications*, 50(8-9):1425 – 1442, 2005. 9

[42] Bryan S. Morse, Terry S. Yoo, Penny Rheingans, David T. Chen, and K. R. Subramanian. Interpolating implicit surfaces from scattered surface data using compactly supported radial basis functions. In *ACM SIGGRAPH 2005 Courses*, SIGGRAPH '05, New York, NY, USA, 2005. ACM. 8, 9

[43] C.T. Mouat and R.K. Beatson. RBF Collocation. Technical Report UCDMS2002/3, Department of Mathematics & Statistics, University of Canterbury, New Zealand, February 2002. 9, 10, 14

[44] Jia Pan and Dinesh Manocha. Fast GPU-based Locality Sensitive Hashing for K-Nearest Neighbor Computation. *Proceedings of the 19th ACM SIGSPATIAL GIS '11*, 2011. 28

[45] Robert Schaback. Multivariate Interpolation and Approximation by Translates of a Basis Function. In C.K. Chui and L.L. Schumaker, editors, *Approximaton Theory VIII–Vol. 1: Approximation and Interpolation*, pages 491–514. World Scientific Publishing Co., Inc, 1995. 4, 10, 19

[46] J. Schmidt, C. Piret, B.J. Kadlec, D.A. Yuen, E. Sevre, N. Zhang, and Y. Liu. Simulating Tsunami Shallow-Water Equations with Graphics Accelerated Hardware (GPU) and Radial Basis Functions (RBF). In *South China Sea Tsunami Workshop*, 2008. 30

[47] J. Schmidt, C. Piret, N. Zhang, B.J. Kadlec, D.A. Yuen, Y. Liu, G.B. Wright, and E. Sevre. Modeling of Tsunami Waves and Atmospheric Swirling Flows with Graphics Processing Unit (GPU) and Radial Basis Functions (RBF). *Concurrency and Computat.: Pract. Exper.*, 2009. 9, 30

[48] C. Shu, H. Ding, and K. S. Yeo. Local radial basis function-based differential quadrature method and its application to solve two-dimensional incompressible Navier-Stokes equations. *Computer Methods in Applied Mechanics and Engineering*, 192(7-8):941 – 954, 2003. 9, 19

[49] C Shu, H Ding, and N Zhao. Numerical Comparison of Least Square-Based Finite-Difference (LSFD) and Radial Basis Function-Based Finite-Difference (RBFFD) Methods. *Computers and Mathematics with Applications*, 51(8):1297–1310, 2006. 9, 10, 19

[50] D Stevens, H Power, M Lees, and H Morvan. The use of PDE centres in the local RBF Hermitian method for 3D convective-diffusion problems. *Journal of Computational Physics*, 2009. 7, 9, 10, 16, 19

[51] David Stevens, Henry Power, Michael Lees, and Herve Morvan. A Meshless Solution Technique for the Solution of 3D Unsaturated Zone Problems, Based on Local Hermitian Interpolation with Radial Basis Functions. *Transp Porous Med*, 79(2):149–169, Sep 2008. 9, 10, 16

[52] David Stevens, Henry Power, and Herve Morvan. An order-N complexity meshless algorithm for transport-type PDEs, based on local Hermitian interpolation. *Engineering Analysis with Boundary Elements*, 33(4):425 – 441, 2008. 9, 10, 16, 30

[53] A. I. Tolstykh and D. A. Shirobokov. On using radial basis functions in a "finite difference mode" with applications to elasticity problems. In *Computational Mechanics*, volume 33, pages 68 – 79. Springer, December 2003. 19

[54] A.I. Tolstykh. On using RBF-based differencing formulas for unstructured and mixed structured-unstructured grid calculations. In *Proceedings of the 16 IMACS World Congress, Lausanne*, pages 1–6, 2000. 18, 19

[55] Robert Vertnik and Božidar Šarler. Meshless local radial basis function collocation method for convective-diffusive solid-liquid phase change problems. *International Journal of Numerical Methods for Heat & Fluid Flow*, 16(5):617–640, 2006. 9, 16

[56] B. Šarler and R. Vertnik. Meshfree Explicit Local Radial Basis Function Collocation Method for Diffusion Problems. *Computers and Mathematics with Applications*, 51(8):1269–1282, 2006. 9, 16

[57] J. G. Wang and G. R. Liu. A point interpolation meshless method based on radial basis functions. *Int. J. Numer. Methods Eng.*, 54, 2002. 9

[58] Grady Wright and Bengt Fornberg. Scattered node mehrstellenverfahren-type formulas generated from radial basis functions. In *The International Conference on Computational Methods*, December 15-17 2004. 9, 19

[59] Grady B. Wright. *Radial Basis Function Interpolation: Numerical and Analytical Developments*. PhD thesis, University of Colorado, 2003. 9, 19, 21

[60] Grady B. Wright, Natasha Flyer, and David A. Yuen. A hybrid radial basis function–pseudospectral method for thermal convection in a 3-d spherical shell. *Geochem. Geophys. Geosyst.*, 11(Q07003):18 pp., 2010. 3, 8, 9, 16, 25

[61] Grady B. Wright and Bengt Fornberg. Scattered node compact finite difference-type formulas generated from radial basis functions. *J. Comput. Phys.*, 212(1):99–123, 2006. 9, 11, 19, 21

[62] Z M Wu. Hermite-Birkhoff interpolation of scattered data by radial basis functions. *Approx. Theory Appl*, (8):1–10, 1992. 7

[63] Xuan Yang, Zhixiong Zhang, and Ping Zhou. Local Elastic Registration of Multimodal Medical Image Using Robust Point Matching and Compact Support RBF. In *BMEI '08: Proceedings of the 2008 International Conference on BioMedical Engineering and Informatics*, pages 113–117, Washington, DC, USA, 2008. IEEE Computer Society. 9

[64] Rio Yokota, L.A. Barba, and Matthew G. Knepley. PetRBF — A parallel O(N) algorithm for radial basis function interpolation with Gaussians. *Computer Methods in Applied Mechanics and Engineering*, 199(25-28):1793–1804, May 2010. 30

[65] Hao Zhang and Marc G. Genton. Compactly supported radial basis function kernels, 2004. 9